HIGH CYCLE FATIGUE STRENGTH OF DISSIMILAR WELDED ROTOR STEELS AT MODERATE TEMPERATURE

M.L. Zhu, F.Z. Xuan
Key Laboratory of Safety Science of Pressurized System, MOE; School of Mechanical Engineering, East China University of Science and Technology, 200237 Shanghai, PR China

High cycle fatigue (HCF) strength of dissimilar welded rotor steels was investigated under axial loading for lifetime of 5×10^7 cycles in air at 25 °C and 370 °C. Scanning Electronic Microscopy (SEM) was utilized to characterize fractured surface. Results show that the largest fatigue strength occurs in upper side SAW at 25 °C while TIG has the lowest fatigue strength at 370 °C. Subsurface crack initiation with fish-eyes were observed on all fractured surfaces but without fine granular area (FGA). The changing of fatigue strength was rationalized by temperature influence and different crack initiation mechanisms in SAW and TIG, where cracks initiated from internal inclusions and porosities, respectively. Welding pores are more detrimental to fatigue life.

Keywords: Very high cycle fatigue; fatigue strength; rotor steels; dissimilar welding

1 INTRODUCTION

In many industries, the required design lifetime often exceeds 10^8 cycles. The traditional safe-life design based on infinite-life criterion has been challenged with the continuous decreasing stress-life response when fatigue cycles beyond 10^7 cycles in many materials, where the fatigue limit cannot display [1]. Recently, the concept of competing modes of fatigue failure [2, 3] has been introduced to emphasize the importance to improve the life design methods. During the past few years, very high cycle fatigue (VHCF) has been widely investigated, and it has been generally established that fatigue failure can occur over 10^7 cycles and is always related to subsurface initiated cracks leading to final fracture [4-6].

A variety of materials were used to understand VHCF mechanisms, such as high-strength steels [6], cast irons [7] and cast aluminums [8]. However, little study uses welding joint. Petit et al. [9] reviewed the influence of atmosphere environment on the VHCF behavior by taking into account of air humidity, degree of vacuum, and most importantly, the air temperature. Up to now, effect of temperature on VHCF behavior is still short of investigation. The available literatures are mainly focused on reporting VHCF properties leaving the crack initiation and growth mechanisms incompletely elucidated [10-12]. Therefore, it is quite significant to examine the VHCF properties of weld joint at high temperatures.

In this work, HCF strength of dissimilar welded rotor steels were investigated at room and moderate temperatures. Scanning Electronic Microscopy (SEM) was utilized to characterize fracture surface. Effects of temperature and welding method on fatigue strength and fracture mechanisms in the very high cycle regime were highlighted.

2 MATERIALS AND EXPERIMENTS

Two rotor steels, i.e., 23CrMoNiWV88 and 26NiCrMoV145 were butt-welded by tungsten inert gas (TIG) welding at the bottom and submerged arc welding (SAW) at the top (Fig. 1). The chemical compositions of the dissimilar welding base metals are shown in Table 1. Mechanical properties of IP and LP are listed in Table 2. Post weld heat treatment was performed at 620 °C for 10 h. In this research, specimens for VHCF tests were cut off from both the SAW and TIG welding parts in the radical direction (includes upper and lower sides), as depicted in Fig. 1. Fig. 2 shows the schematic of VHCF specimens.

Fatigue tests were carried out at 25 °C and 370 °C under axial loading at R= -1. Different stress levels were chosen in an attempt to cycle 5×10^7 cycles to obtain endurance strength. After testing, fracture surfaces of failed specimens were characterized by SEM.

Materials	C	Si	Mn	P	S	Ni	Cr	Mo	V	Sn	As	Sb
23CrMoNiWV88	0.23	0.06	0.70	0.006	0.002	0.74	2.09	0.82	0.29	0.005	0.005	0.0013
26NiCrMoV145	0.25	0.04	0.29	0.005	0.001	3.56	1.71	0.38	0.09	0.003	0.004	0.0013

Table 1: Chemical composition (wt.%) of base metals of the welding joint

Materials	Yield strength $\sigma_{0.2}$, MPa	Ultimate tensile strength σ_b, MPa	Elongation δ, %	Reduction of area ψ, %
23CrMoNiWV88	703	816	19	74
26NiCrMoV145	835.5	938	20	73

Table 2: Mechanical properties of base metals of the welding joint

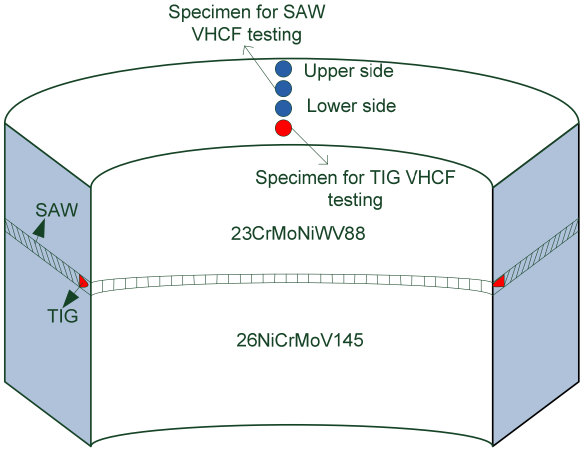

Fig. 1: Schematic of specimen preparation from the dissimilar welding joint

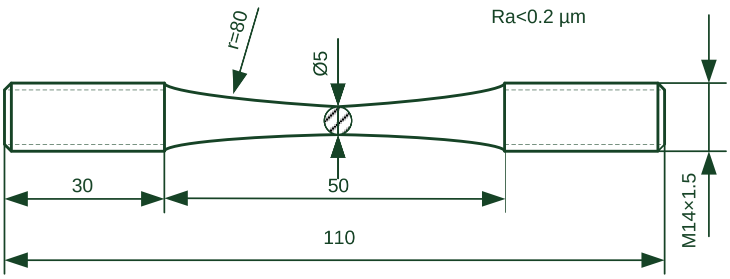

Fig. 2: Schematic of VHCF test specimen

3 RESULTS AND DISCUSSION

3.1 S-N characteristics

Fig. 3 shows the stress amplitude σ_a versus number of cycles to failure N_f of VHCF tests at

25 °C and 370 °C. The endurance strength at 25 °C in upper side SAW at 5×10^7 cycles approaches 360 MPa. Fatigue strength at 5×10^7 cycles are decreased at 370°C, regardless of the weld methods and specimen locations. Interestingly, endurance strength at lower side SAW which can reach 300 MPa are larger than that in the upper side (around 230 MPa) at 370°C. From Fig. 3, it can be seen that TIG welded specimen may have the lowest fatigue strength at 370°C because all the four specimens fractured without reaching 5×10^7 cycles.

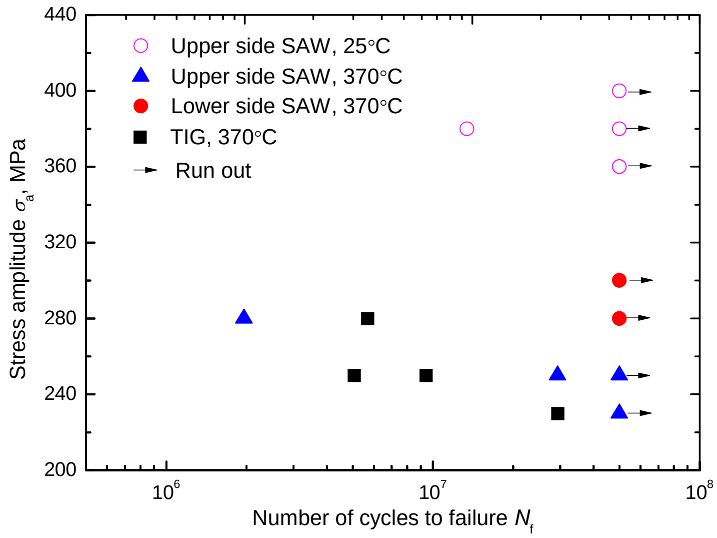

Fig. 3: S-N data (σ_a versus N_f)

3.2 SEM observations of fracture surface

Fig. 4 shows fracture surface of the specimen tested at 25 °C in the upper side SAW. In Fig. 4a, three zones exist on the surface, including a fish-eye feature, stable crack growth zone and final fracture zone. It is apparent that crack initiates from the inclusion (Fig. 4b). Energy Dispersive Spectrometer (EDS) analysis shows that chemical composition of the inclusion are rich in Ca, Mg, Al and Si. In the stable crack growth zone (Fig. 4c), small fatigue striations can be observed. Interestingly, the popular characteristics around the inclusion in VHCF such as optically dark area (ODA) by Murakami et al. [13], granular bright facet (GBF) by Shiozawa et al. [4] and FGA (fine granular area) by Sakai et al. [14] cannot be observed in a magnified micrograph of the inclusion, as depicted in fig.4d. The surface without FGA may be related to the lower fatigue cycles [13], here the N_f only reaches 13,398,314 cycles.

Fig. 5 shows fracture surface of the specimen tested at 370 °C (σ_a=250 MPa, N_f=29,307,156 cycles) in the upper side SAW. The crack was also initiated from the inclusion thus forming the fish-eye, and Ca, Mg, Al and Si are the main chemical composition. It is interesting to find that another inclusion (Fig. 5a) also exists on the surface, but this inclusion cannot initiate cracks for further growth. By comparing with Fig. 4b, it can be seen that the fish-eye zone which shows a deep color in Fig. 5b clearly differentiates from the crack growth zone. In the crack growth zone (Fig. 5c), many fine striations can be observed. A magnified micrograph of fish-eye in fig.5d shows that FGA is also not observed around the inclusion, which means that 3×10^7 cycles may be still short [13]. From Fig. 4 and Fig. 5, it can be seen that non-metallic inclusions are the initiation site, and the fish-eye feature always locates near surface.

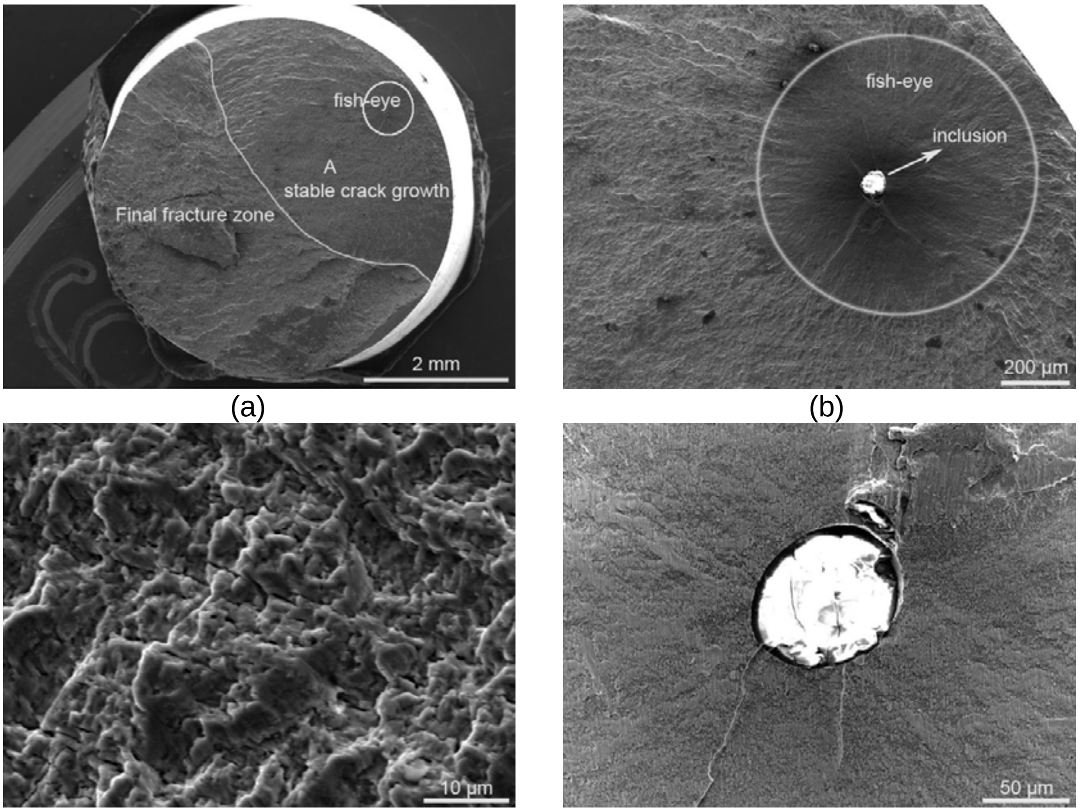

(a) (b) (c) (d)

Fig. 4: Fracture surface observation of the specimen tested at 25 °C (σ_a=380 MPa, N_f=13,398,314 cycles) in the upper side SAW: (a) three different zones, (b) fish-eye feature, (c) fatigue striations at ‘A’ in (a), and (d) a magnified micrograph of fish-eye in (b).

As for TIG, all the four specimens failed in weld metal. Fig. 6 indicates the fracture surface observation results of the specimen tested at 370 °C. The specimen sustained 5,686,569 cycles at stress amplitude of 280 MPa. In fig.6a, it can be seen that many porosities are present on the fracture surface, such as A, B, C, D and E. Micrographs showing the porosities in detail are illustrated in Figs. 6b-e. Two fish-eyes can be observed in Fig. 6b which contains porosities A and B. The cracks are initiated from both A and B, but only A forms the main crack for further propagation (Fig. 6b). Figs. 6c-e shows the porosities C, D and E, respectively. Ductile dimples can be observed around the porosity C (Fig. 6c) while fatigue striations exist close to the porosity D (Fig. 6d). The different character around porosities C and D can be related to their position relative to the initiation zone. For example, the location of C is in the final fracture zone, whereas D locates in the crack growth zone. Therefore, it would be not difficult to find that fatigue striations occur mostly at ‘2’ (Fig. 6g) while less striations can be found at ‘1’ (Fig. 6f). It is also worth noting that interface appears near the final fracture zone (Fig. 6h), which marks the changing of rough ridges to smooth surface.

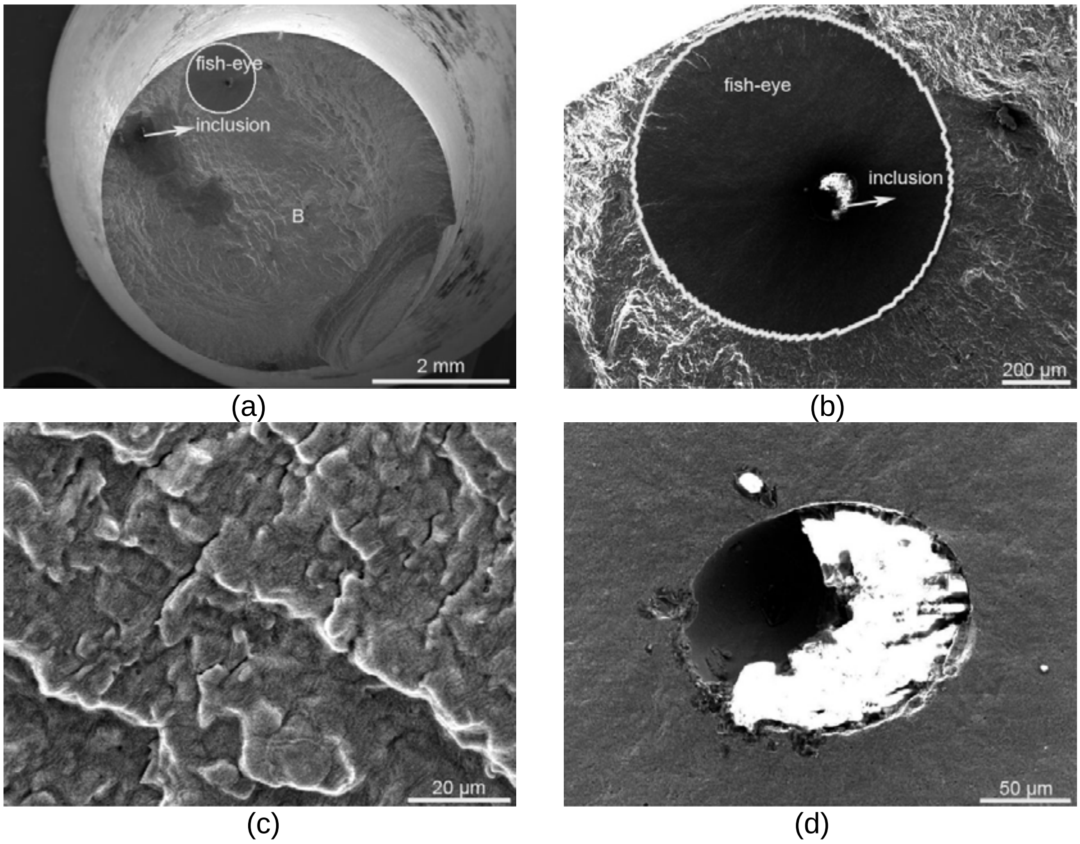

Fig. 5: Fracture surface observation of the specimen tested at 370 °C (σ_a=250 MPa, N_f=29,307,156 cycles) in the upper side SAW: (a) macrograph of fracture surface, (b) fish-eye feature, (c) fracture mode at ‘B’ in (a), and (d) a magnified micrograph of fish-eye in (b).

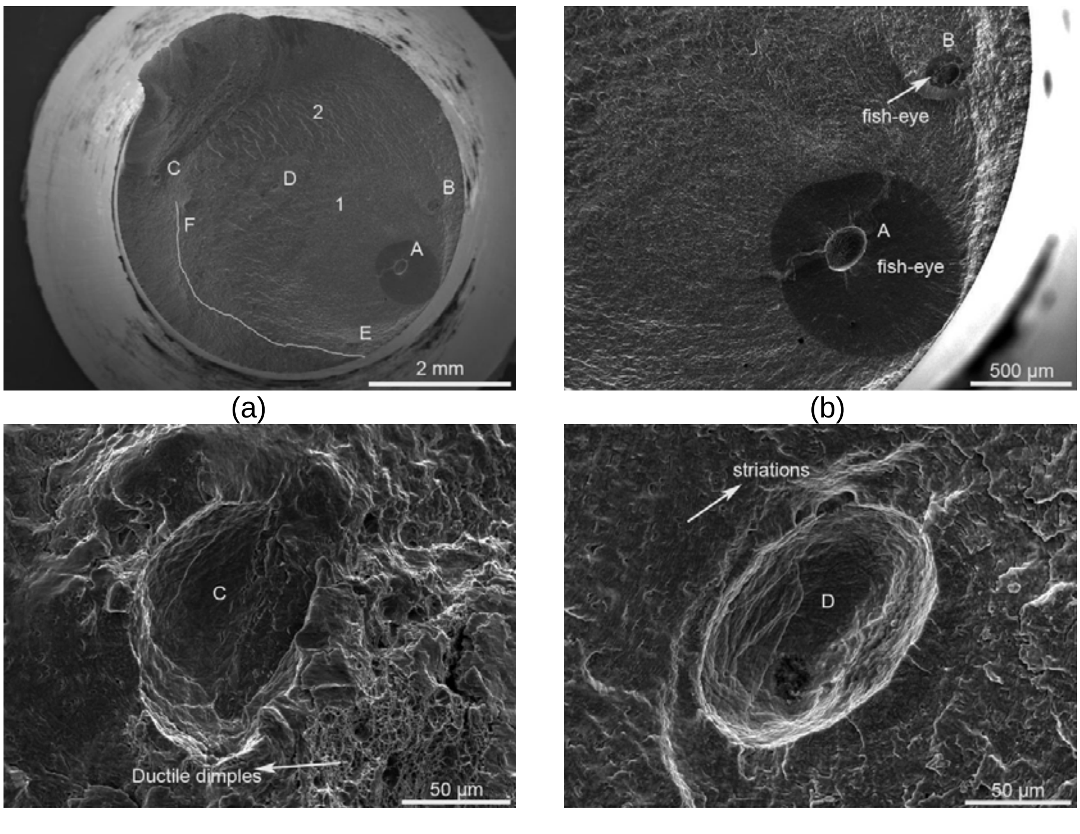

(c) (d)

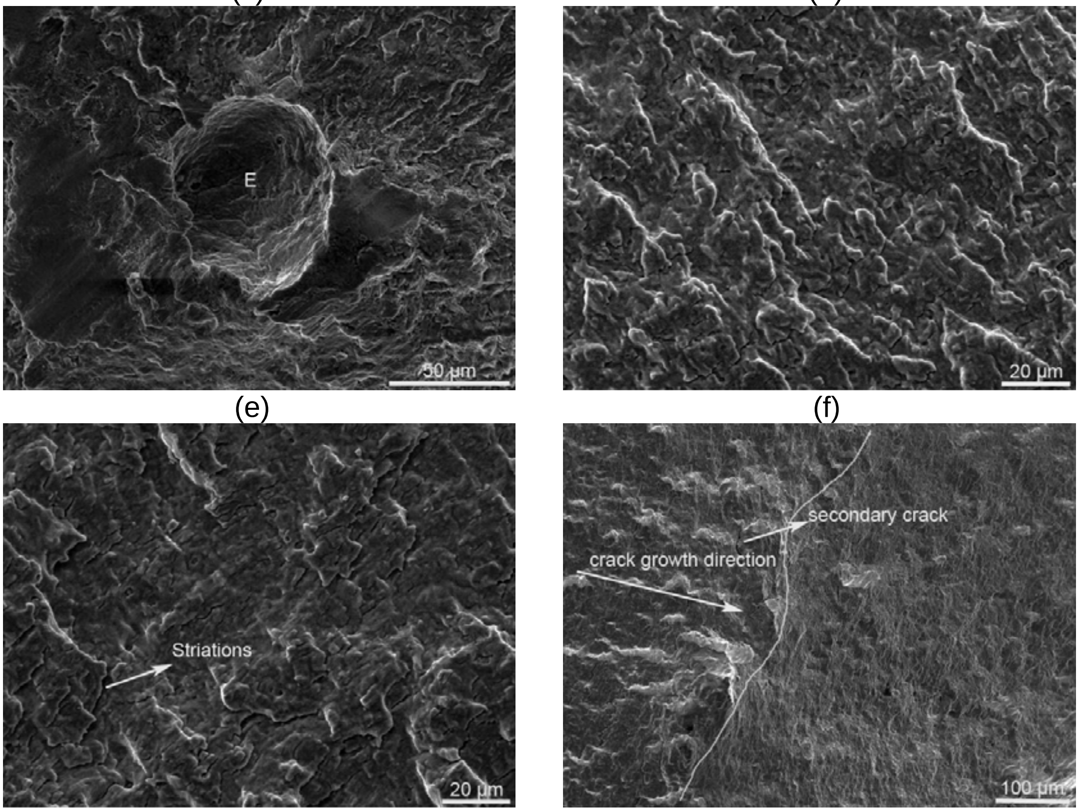

(g) (h)

Fig. 6: Fracture surface observation of the specimen tested at 370 °C (σ_a=280 MPa, N_f=5,686,569 cycles) in TIG: (a) macrograph of fracture surface, (b) fish-eye feature of porosity A and B, (c) porosity C with ductile dimples around, (d) porosity D with striations around, (e) porosity E, (f) fracture mode at ‘1’ in (a), (g) fracture mode at ‘2’ in (a), and (h) microscopic observation of interface at ‘F’ in (a).

3.3 Temperature and welding method dependence of fatigue strength

As mentioned before, although the fatigue cycle is not very high, sub-surface initiated fish-eye occurs on every fractured specimen at both 25 °C and 370 °C, regardless of welding methods. Fatigue strength in upper side SAW at 25 °C is 130 MPa higher than that at 370 °C. Therefore, it seems that test temperature plays an important role in fatigue properties. Another interesting point should be mentioned is that for the same test temperature, fatigue strength of TIG welded specimen are lower than those of SAW, and fatigue strength in upper side SAW are lower than that in lower side. It is worth noting that fatigue cracks initiate from non-metallic inclusions in all the SAW specimens, but it changes to welding defects such as porosity in all the TIG specimens. This further indicates that fatigue strength also shows a welding method dependent trend.

Kawagoishi et al. [15] concluded that the change of fatigue strength at higher temperatures is dependent on the competition between the softening of matrix and the surface oxidation process. Similar results show that fatigue strength of smooth specimens at elevated temperatures up to 600 °C was higher than that at room temperature due to the oxidation induced suppression of crack initiation and small crack growth [12]. In this work, it would be expected that material oxidation has a lower influence on the initiation and propagation of surface cracks at moderate temperatures, although the appearance of fish-eyes in figs. 5 and 6 are more distinctive to the crack growth zones. Therefore, it can be concluded that the softening of the material may play a decisive role in the decreasing of fatigue strength at 370 °C.

The influence of microstructure can be introduced to explain why fatigue strength in the lower side SAW is higher than that in the upper side. During the past few years, the relationship between fatigue strength and inclusion size has been gradually emphasized [16, 17]. It is reasonable to conclude that microstructures in the upper side SAW would be larger than those in the lower side, where the microstructures are normalized in a multi-layer welding process [18]. As a result of the easiness to initiate fatigue cracks in materials with larger inclusions, it is convincing that the larger the inclusion size, the lower the fatigue strength. In order to elucidate the distribution of inclusion size along the SAW weld joint, further VHCF tests should be conducted.

The initiation of fatigue cracks at porosities in TIG can provide important information to optimize welding parameters. Crack initiation in porosity has also been found in cast iron [7, 8] and cast aluminum [8] in the very high cycle regime. It is reasonable that TIG welded specimens have the lowest fatigue strength because it is easier to initiate fatigue cracks in pores where the atomic binding force is lower.

It is interesting to find that although the crack initiation mechanisms are different between upper side SAW and TIG specimens, the fatigue strength of them at 370 °C are close to each other. It has been generally accepted that a large portion of fatigue life is occupied by crack initiation in the long life regime. Further work should be made to establish the probable relationship between the pores and inclusion size. On the other hand, of the two types of defects (inclusion and pores), it is reasonable to conclude that the pores in the microstructure are more detrimental to fatigue life.

4 CONCLUSION

HCF strength of dissimilar welded rotor steels was investigated under axial loading at room and moderate temperatures. The main conclusions are listed as follows:

(1) Fatigue strength decreased at 370 °C when comparing with that at 25 °C, and it is also influenced by welding methods.
(2) Subsurface crack initiations with fish-eyes but without FGA are observed on all fractured surfaces. Cracks initiate from internal inclusion in SAW while welding porosities are the initiation site in TIG specimens.
(3) Of the two types of defects (inclusions and porosity), porosities in the microstructure are more detrimental to fatigue life.

ACKNOWLEDGEMENTS

The authors are grateful for the supports provided by National Natural Science Foundations of China (50835003, 10972078). FZ would also wish to thank the Research Fund for Doctoral Program of Higher Education (200802510003) and Natural Science Foundation of Shanghai (09JC1404400).

REFERENCE

[1] Marines I, Bin X, Bathias C. An understanding of very high cycle fatigue of metals. International Journal of Fatigue 2003;25(9-11):1101-1107.
[2] Cashman GT. A review of competing modes fatigue behavior. International Journal of Fatigue 2010;32(3):492-496.
[3] Chandran KSR, Chang P, Cashman GT. Competing failure modes and complex *S-N* curves in fatigue of structural materials. International Journal of Fatigue 2010;32(3):482-491.
[4] Shiozawa K, Lu L. Very high-cycle fatigue behavior of shot-peened high-carbon-chromium bearing steel. Fatigue & Fracture of Engineering Materials & Structures 2002;25(8-9):813-822.
[5] Carstensen JV, Mayer H, Brondsted P. Very high cycle regime fatigue of thin walled tubes made from austenitic stainless steel. Fatigue & Fracture of Engineering Materials & Structures 2002;25(8-9):837-844.
[6] Nie YH, Fu WT, Hui WJ, Dong H, Weng YQ. Very high cycle fatigue behavior of 2000-MPa ultra-high-strength spring steel with bainite-martensite duplex microstructure. Fatigue & Fracture of Engineering Materials & Structures 2009;32(3):189-196.
[7] Wang QY, Berard JY, Dubarre A, Baudry G, Rathery S, Bathias C. Gigacycle fatigue of ferrous alloys. Fatigue & Fracture of Engineering Materials & Structures 1999;22(8):667-672.
[8] Bayraktar E, Garcias IM, Bathias C. Failure mechanisms of automotive metallic alloys in very high cycle fatigue range. International Journal of Fatigue 2006;28(11):1590-1602.
[9] Petit J, Sarrazin-Baudoux C. An overview on the influence of the atmosphere environment on ultra-high-cycle fatigue and ultra-slow fatigue crack propagation. International Journal of Fatigue 2006;28(11):1471-1478.
[10] Kobayashi H, Todoroki A, Oomura T, Sano T, Takehana T. Ultra-high-cycle fatigue properties and fracture mechanism of modified 2.25Cr-1Mo steel at elevated temperatures International Journal of Fatigue 2006;28(11):1633-1639.
[11] Miao J, M.Pollock T, Jones JW. Crystallographic fatigue crack initiation in nickel-based superalloy René 88DT at elevated temperature. Acta Materialia 2009;57(20):5964-5974.
[12] Kawagoishi N, Chen Q, Yan N, Goto M, Wang Q, Ohzono Y. Fracture mechanism in fatigue of Nickel-based superalloy inconel 718 at elevated temperatures. Journal of Solid Mechanics and Materials Engineering 2007;1(6):734-743.
[13] Murakami Y, Yokoyama NN, Nagata J. Mechanism of fatigue failure in ultralong life regime. Fatigue & Fracture of Engineering Materials & Structures 2002;25(8-9):735-746.
[14] Sakai T, Sato Y, Oguma N. Characteristic S-N properties of high-carbon-chromium-bearing steel under axial loading in long-life fatigue. Fatigue & Fracture of Engineering Materials & Structures 2002;25(8-9):765-773.
[15] KAWAGOISHI N, CHEN Q, NISITANI1 H. Fatigue strength of Inconel 718 at elevated temperatures. Fatigue & Fracture of Engineering Materials & Structures 2000;23(3):209-216.
[16] Ishii H, Yagasaki T, Akagi H. Evaluation of giga-cycle fatigue properties of some maraging steels by intermittent ultrasonic fatigue testing. Fatigue & Fracture of Engineering Materials & Structures 2002;25(8-9):831-835.
[17] Liu YB, Yang ZG, Li YD, Chen SM, Li SX, Hui WJ, Weng YQ. Dependence of fatigue strength on inclusion size for high-strength steels in very high cycle fatigue regime. Materials Science and Engineering A 2009;517(1-2):180-184.
[18] Furuya H, aihara S, Morita K. A new proposal of HAZ toughness evaluation method - Part 1: HAZ toughness of structural steel in multilayer and single-layer weld joints. Welding Journal 2007;86(1):1S-8S.